Triple point fermions in ferroelectric GeTe

Juraj Krempaský[1], Laurent Nicolaï[2], Martin Gmitra[3], Houke Chen[4], Mauro Fanciulli[5], Eduardo B. Guedes[1],
Marco Caputo[1], Milan Radović[1], V. V. Volobuev[6,7], Ondřej Caha[8], Gunther Springholz[9], Jan Minár[2], and J. Hugo Dil[1,10]

[1]*Photon Science Division, Paul Scherrer Institut,*
CH-5232 Villigen, Switzerland
[3]*New Technologies-Research Center University of West Bohemia,*
Plzeň, Czech Republic
[3]*Institute of Physics, P. J. Šafárik University in Košice,*
Park Angelinum 9, 040 01 Košice, Slovakia
[4]*Department of Physics,*
Tsinghua University, Beijing 100084, China
[5]*LPMS, Université de Cergy-Pontoise,*
95031 Cergy-Pontoise, France
[6]*International Research Centre MagTop,*
Institute of Physics, Polish Academy of Sciences,
Aleja Lotnikow 32/46, PL-02668 Warsaw, Poland
[7]*National Technical University "KhPI",*
Kyrpychova Str. 2, 61002 Kharkiv, Ukraine
[8]*Department of Condensed Matter Physics,*
Masaryk University, Kotlářská 267/2,
61137 Brno, Czech Republic
[9]*Institut für Halbleiter-und Festkörperphysik,*
Johannes Kepler Universität, A-4040 Linz, Austria
[10]*Institut de Physique, École Polytechnique Fédérale de Lausanne,*
CH-1015 Lausanne, Switzerland

(Dated: October 30, 2021)

Ferroelectric α-GeTe is unveiled to exhibit an intriguing multiple non-trivial topology of the electronic band structure due to the existence of triple-point and type-II Weyl fermions, which goes well beyond the giant Rashba spin splitting controlled by external fields as previously reported. Using spin- and angle-resolved photoemission spectroscopy combined with ab initio density functional theory, the unique spin texture around the triple point caused by the crossing of one spin degenerate and two spin-split bands along the ferroelectric crystal axis is derived. This consistently reveals spin winding numbers that are coupled with time reversal symmetry and Lorentz invariance, which are found to be equal for both triple-point pairs in the Brillouin zone. The rich manifold of effects opens up promising perspectives for studying non-trivial phenomena and multi-component fermions in condensed matter systems.

The exploration of topological materials commenced with the discovery of topological insulators [1–10], followed by topological semimetals [11–14], topological superconductors [15] and nodal line semimetals [16]. Recently, topological semimetals with triply-degenerate points were predicted in materials such as molybdenum phosphide [17], tungsten carbide [18], InAs$_{1-x}$Sb$_x$ alloys [19], and strained HgTe [20]. In contrast to an even number of band crossings, band structures with triple band crossing are rather rare in condensed matter. Such triple-point (TP) fermions can be found along the high symmetry axis in the Brillouin zone (BZ) allowing for two and one dimensional double group representations [19, 21, 22]. This is also the case for α-GeTe(111) which was so far extensively studied in terms of the topologically trivial Rashba-type band structure [23–25].

The origin of these intriguing features in α-GeTe lies in the spontaneous structural phase transition of the inversion symmetric rock-salt β-GeTe structure (FCC, space group #225) into a ferroelectric rhombohedral structure with Ge-atoms displaced by ≈ 0.3 Å and distorted by $\approx 2°$ (space group #160) [24, 26]. This inversion symmetry breaking introduces a

spin-splitting except for the bands that line up with the high-symmetry ferroelectric $\langle 111 \rangle$ axis, which is the main symmetry axis of the C_{3v} point group. Along this axis TP fermions can form which are classified as type-A or B, depending on the number of nodal lines that connect a pair of TP.

In this Letter we provide theoretical and experimental evidence that α-GeTe possess type-B triple point fermions inside its valence band states along the ferroelectric $\langle 111 \rangle$ axis. To this date such non-trivial topology in α-GeTe failed to be noticed. The spin texture around the TP is unravelled and the same spin winding number of ± 1 is found for both TP pairs in the 3D BZ. Furthermore, we identified additional Dirac and type-II Weyl fermions that coexist with these three-component fermions.

Epitaxial films of 200 nm of α-GeTe for our (spin-) and angle-resolved photoemission spectroscopy ((S)ARPES) studies were grown by molecular beam epitaxy on BaF$_2$(111) substrates and in situ transferred for high-resolution ARPES at the UE112-PGM2a beamline of BESSY II. SARPES measurements were performed at the Swiss Light Source of the Paul Scherrer Institut at the COPHEE end station equipped
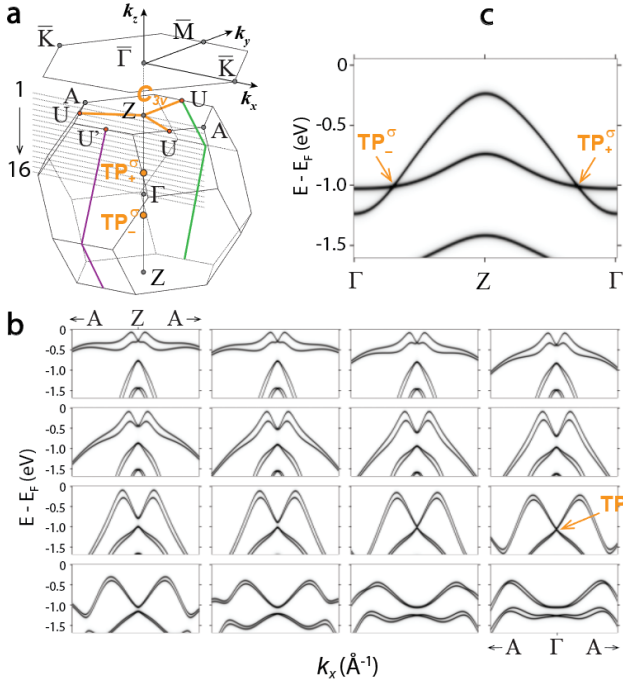
FIG. 1. (a) Bulk BZ and surface BZ of rhombohedral α-GeTe with $\langle 111\rangle$ ferroelectric axis along the k_z direction. (b) BSF initial state calculations along k_x for sixteen selected k_z values denoted in panel (a). (c) Band structure along k_z with position of TP^σ_- and TP^σ_+ indicated by orange arrows.

is a Dirac point (DP) near 2 eV binding energy. Second, a type-II Weyl point (WP II) appears around -0.4 Å^{-1} as indicated in the figure. The presence of this Weyl point influences the spin texture and changes the spin winding number from ± 1 to ± 2, as seen in Fig. 5e,f and discussed in more detail below.

Following the TP-classification by Winkler $et\ al.$[21], α-GeTe should host a type-B TP with four nodal lines. Fig. 2 summarizes this scenario: panel (b) resolves the bands $\Lambda_{4,5,6}$ dispersing in k_z, whereby the two spin-split bands Λ_4, Λ_5 cross the doubly degenerate Λ_6, forming a pair of triple fermion quasiparticles. In contrast to type-A TPs with only one nodal line, the triple points within each pair TP^σ_- and TP^σ_+ are connected by four nodal lines. One nodal line is lined up with the C_{3v} axis and therefore shows up at zero in-plane momentum only (purple markers in Fig. 2c-e). On the other hand the three remaining nodal lines are extending in three vertical mirror planes, which in our case line up along
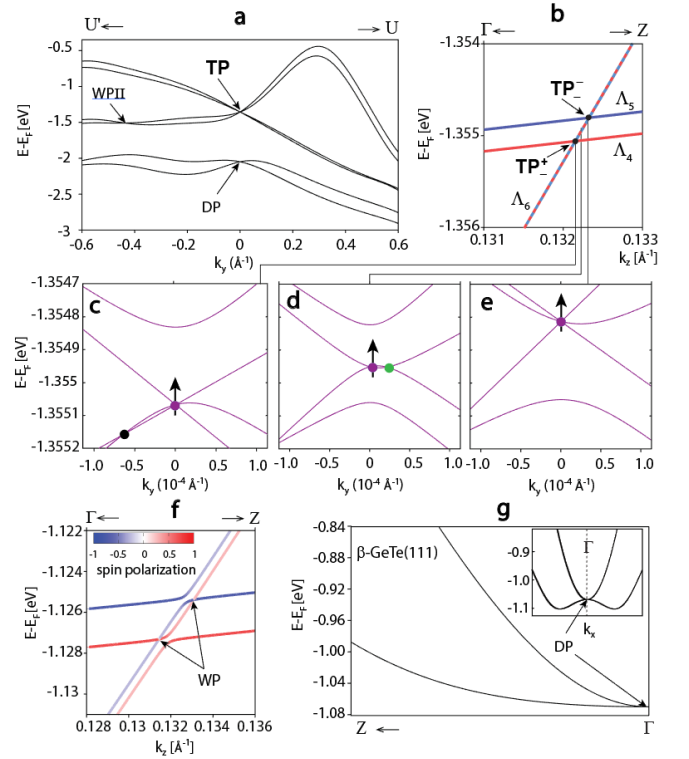
with two orthogonal Mott polarimeters to measure the three spatial components of spinors in arbitrary reciprocal space points [27]. We compared our experimental data with calculated initial state band-maps presented in terms of Bloch spectral functions (BSF) as implemented in the fully relativistic spin-polarised Korringa-Kohn-Rostoker theory [28] and with the full potential all-electron Wien2K density functional code. Considering the relatively small energy scales involved, this allowed us to check the results for consistency.

Fig. 1a shows the BZ with two pairs of triple points TP^σ_z, where the $\sigma = \pm$ index denotes the TP within a single pair, and $z = \pm$ denotes the two TP pairs with opposite k_z within the BZ. Panel (b) shows valence band (VB) dispersions for sixteen selected k_z values in the Z-A-Γ plane. The top-left image presents the Rashba-type spin splitting of the uppermost VB at the Z-point. When moving k_z towards Γ these bands disperse and finally meet with the lower spin-split bands at approximately $\frac{1}{3}$BZ distance from the Γ-point (orange arrow). Another visualization of the TP formation is in panel (c) plotting the dispersion along ΓZ. At first glance this crossing point is reminiscent of the topologically protected touching point between electron and hole pockets in a double-Weyl scenario[29–31], but Fig. 2b-e unambiguously resolve a three-component fermion matching the space group symmetry. Besides this, the bulk electronic structure in the U'-Z-U mirror plane for a k_z right at the TP in Fig. 2a shows two additional band crossings with non-trivial topology. First, there

FIG. 2. (a) Calculated band structure along the U'-Z-U mirror plane, with triple point (TP), type-II Weyl fermion (WP II) and Dirac point (DP). (b) Formation of TP pair (TP^-_-, TP^+_-) by spin-degenerate band Λ_6 and two spin split bands $\Lambda_{4,5}$. (c,d,e) Close-up of band structure along k_y at three different values of k_z across the TP pair. Three types of touching points are indicated with black, green, and magenta markers, black arrows indicate the k_z dispersion of the latter. (f) Band structure around the TP under 10 T B-field along the z-direction. The TP splits into a pair of Weyl points (WP). (g) Band structure for rock-salt β-GeTe above ferroelectric phase transition. The triple fermions merges into a single Dirac point (DP). (inset) band structure along k_x.
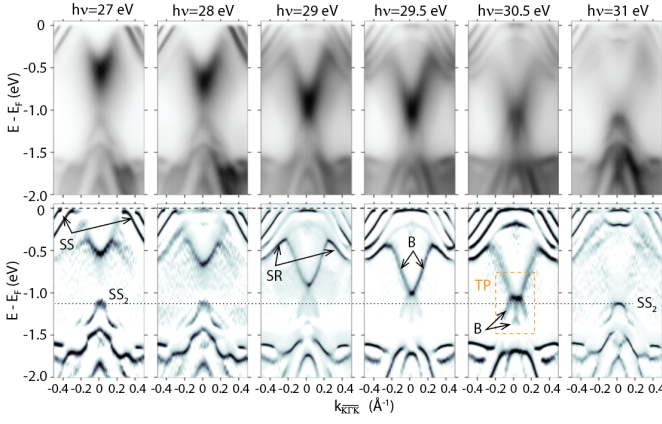
FIG. 3. (top) High-resolution ARPES data for various photon energies around the TP. (bottom) Corresponding curvature maps showing the TP formation at 30.5 eV photon energy inside the orange frame. The arrows indicate surface states SS, SS_2, surface resonances (SR) and bulk bands (B).

the three Z-U directions (orange lines in Fig. 1a). Panels (c-e) are close-ups of the bands structure across the single $TP^\pm_-$ pair for three k_z values. For the intermediate k_z between TP^-_- and TP^+_- there are two crossing points forming two of the four nodal lines, whereby the one at finite $k_\parallel$ (black and green markers) disperse with k_z (see animated Figure S1 in Supplemental Material).

As a whole, the triple fermion forms an intermediate state between Dirac and Weyl fermions. Actually, as indicated in Fig. 2f, α-GeTe inside a 10 T magnetic field (which is many orders of magnitude lower than the exchange field in (GeMn)Te [32]) the TP splits into a pair of Weyl points. Furthermore, above the ferroelectric transition temperature ($T_C \approx 700$ K) the TP transforms into a Dirac point as seen in panel (g). This renders GeTe rather unique as all three phases can be achieved under realistic conditions in a single material system.

In our earlier α-GeTe ARPES studies we extensively described the measured electronic structure in terms of surface states (SS), surface resonances (SR), and bulk states (B) [24, 25, 32–34]. Such a decomposition also applies to the ARPES data in Fig. 3 and allows to find the appropriate region for measuring the TP and its spin texture. Below we demonstrate that inside the $-0.2 < k_y < 0.2$ Å^{-1} momentum span the additional spin tag in SARPES data enables us to unambiguously resolve the individual bulk bands around a TP-pair.

Based on the k_z-series of band maps in Fig. 1b, the ARPES data in Fig. 3c, and the schematic k_z vs. photon energy diagram (Supplemental Figure S2), the TP is predicted, and experimentally verified, for photon energies around hν = 30, 58 and 89 eV. The latter two values correspond to consecutive TP pairs at opposite parts of the BZ, thus enabling us to experimentally examine their symmetry connection.

A notable feature of the TP electronic structure is that the bands gradually shift between TP^-_- and TP^+_- as marked by

black arrows in Fig. 2c-e. This spectral weight transfer across the TP is manifested in a series of high-resolution ARPES band maps in Fig. 3c, and their curvature plots [35] in the bottom panels. In accord with the theoretical predictions (Fig. 1b), the k_z-dispersion of the spectral weight is progressing toward the TP around 30.5 eV, where it becomes equally distributed above and below the TP. Interestingly, the band maps inside the orange frame for hν=30.5 eV appear to mimic the TP band mixing seen in Fig. 2c-e, however with much larger momentum and energy scale. Because the bulk spectral intensity around the TP totally suppresses the weakly contributing surface states SS_2 (horizontal dashed line in Fig. 3), the contribution of the latter can be neglected in our SARPES analysis. We note that surface states are typically associated with nodal points in topological metals and semimetals, but SS_2 is not interconnecting the TP pairs because it is clearly off-set in energy at zero momentum, as indicated inside the orange frame. In fact, because both TP pairs line up in the ΓZ-direction, the associated surface states cannot show up on the (111) surface.

Similar to the Rashba model, the spin polarization of bulk states around a TP is expected to be tangentially momentum-locked in accord with time-reversal symmetry (TRS) properties, as also shown in the calculated spin texture in Fig.5e. Our SARPES data is visualized as spin-resolved energy dis-
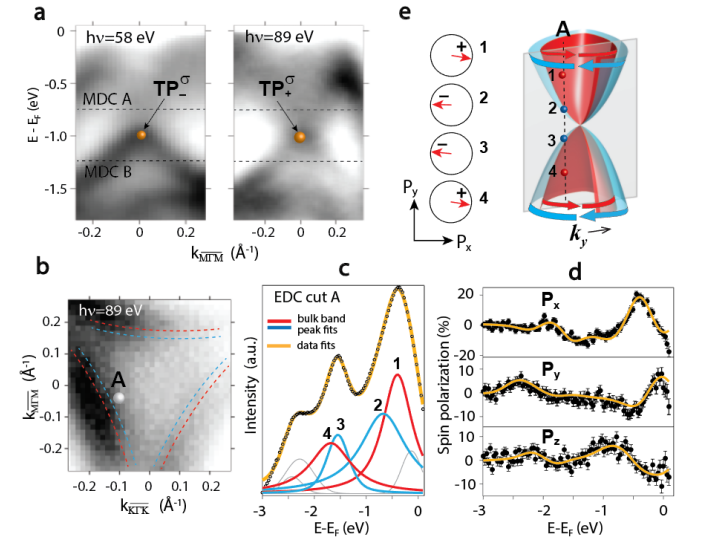

FIG. 4. (a) ARPES band maps along $\overline{M\Gamma M}$ measured at the COPHEE setup with hν=58 and 89 eV. Orange bullets indicate TP^σ_- and TP^σ_+. MDC A and MDC B indicate where data in Fig. 5 is obtained. (b) CEM measured at hν=89 eV and -0.4 eV binding energy at COPHEE. Marker A indicates the $k_{x,y}$ locus used for SARPES EDC, next to the bulk bands denoted with dashed red-blue lines. (c,d) SARPES EDC cut A total intensity and related $P_{x,y,z}$ spin polarizations with corresponding $B_{1,2,3,4}$ bulk band fitting indicated in red-blue and surface-derived bands in gray. (e) 3D TP cartoon illustrating considered EDC cut A with corresponding in-plane spin-textures, showing spin vectors projected mainly along P_x with a characteristic (+ - - +) pattern around the TP.
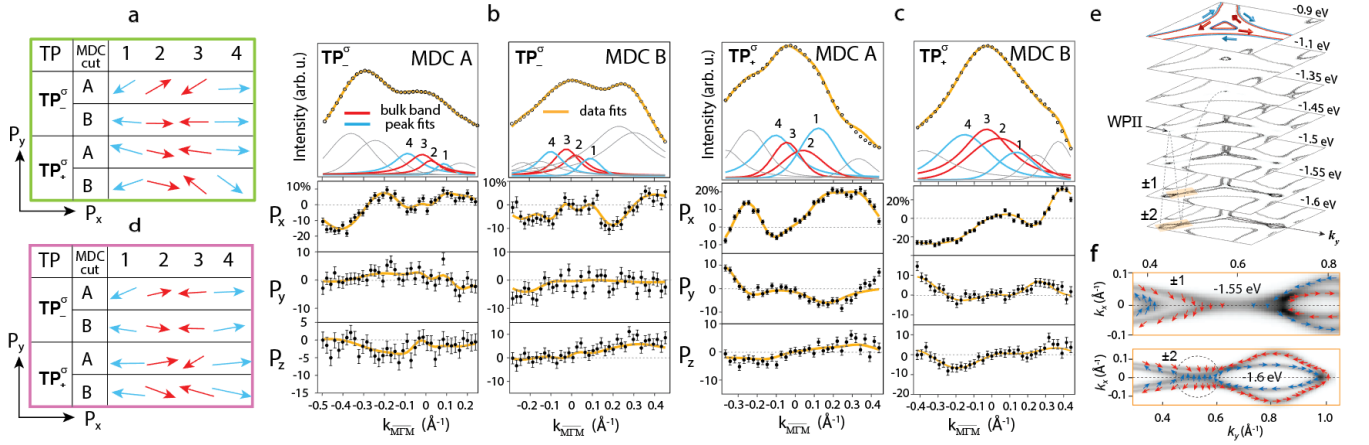
FIG. 5. (a) Tabulated spin textures for TP_-^σ and TP_+^σ measured along the MDC A (MDC B) cuts 250 meV above (below) the TP, as denoted in Fig. 4a. (b,c) Corresponding SARPES intensities and 3D spin polarization fitting for TP_-^σ and TP_+^σ respectively. Red and blue curves indicate the $B_{1,2,3,4}$ peak fitting, surface-derived bands are in gray. (d) Analogous spin textures measured by rotating the sample by 180°, the frames in green and magenta indicate two inequivalent directions denoted in Fig. 1a. (e) BSF constant energy maps, black arrow indicates the Weyl-II fermion, dashed line its energy dispersion and hybridization with TP bands. (f) Close ups of spin-resolved CEMs at -1.55 and -1.6 eV, respectively, showing a change in spin winding number from ±1 to ±2 around the WP II point inclusion with conspicuous "spin swirl" denoted by dashed circle.

tribution (EDC) and momentum distribution curves (MDC) summarized in Figures 4 and 5, respectively. For all measurements our analysis concentrates on the in-plane spin polarisation $P_{x,y}$ of the four spin-split bulk bands denoted by $B_{1,2,3,4}$. Their properties are determined using a 3D vectorial fit of the measured spin expectation values with a well established fitting routine that extracts their positions, widths, intensities, and 3D spin vector [36]. For the EDCs a Shirley background is subtracted from the total intensity, whereas for the MDCs a constant background is used. To simplify comparison between theory and experiment, we aligned the sample in such a way that the out-of-plane spin polarization P_z is oriented along the k_z-direction and P_x (P_y) along the $\overline{\Gamma K}$ ($\overline{\Gamma M}$) direction. Within this experimental geometry a tangential spin winding is determined by P_x.

We first test the spin texture in terms of TRS and Lorentz invariance (LI) for the selected $k_{x,y}$ point labeled A in Fig. 4b, with SARPES data summarized in panels (c-d). The resulting spin texture is summarized in panel (e) next to a model visualizing the EDC cut through the four B_{1-4} bulk bands around the TP. We note that the spin helicity dictated by TRS and LI are preserved: the spins are nearly tangentially locked in momentum, whereby bands $B_{1,4}$ and $B_{2,3}$ do not change the spin helicity. The spin texture imposed by LI, i.e. symmetric spin in energy with regard to the TP, becomes apparent when considering the (+ - - +) pattern in Fig. 4d; in contrast to the Rashba-type (+ - + -) pattern seen in Supplemental Figure S3, measured at the BZ boundary Z-point (see Fig. 1a).

This experimental result is further confirmed in Fig. 5. We measured each TP-pair with two MDC cuts 250 meV above (A) and below (B) the TP, as depicted in Fig. 4a. In addition, because there are two inequivalent directions (Fig. 1a green and magenta lines), each TP-pair was measured along U'-A-U

and after rotation by 180° along U-A-U' (see SARPES data in Supplemental Figure S4). The resulting in-plane spin textures shown in Fig. 5d are consistent with a spin winding number of ±1. To best of our knowledge this is the first experimental evidence of the spin texture of a triple fermion, featuring a winding number of ±1 in accord with both TRS and LI and theoretical predictions. Here it should be noted that the inclusion of WP II induces an additional spin swirl and changes the winding number to ±2 as illustrated by the calculations in Fig. 5e. Furthermore, the two triple point pairs TP_-^σ and TP_+^σ show the same spin helicity in accordance with the absence of a (x, y) mirror plane.

In conclusion, we demonstrated that α-GeTe is a type-B triple fermion topological system enabled by the ferroelectric non-centrosymmetric atomic arrangement of Ge and Te atoms along the ⟨111⟩ axis. Furthermore, we measured for the first time the spin winding number for a triple point system. Moreover, α-GeTe is currently unique in the possibility to manipulate topological properties by temperature variation [24], ferroelectric switching [37], and/or magnetic doping [32].

[1] C. L. Kane and E. J. Mele, Phys. Rev. Lett. **95**, 226801 (2005).

[2] M. Z. Hasan and C. L. Kane, Rev. Mod. Phys. **82**, 3045 (2010).

[3] D. Hsieh, Y. Xia, L. Wray, D. Qian, A. Pal, J. H. Dil, J. Osterwalder, F. Meier, G. Bihlmayer, C. L. Kane, Y. S. Hor, R. J. Cava, and M. Z. Hasan, Science **323**, 919 (2009).

[4] A. Nishide, A. A. Taskin, Y. Takeichi, T. Okuda, A. Kakizaki, T. Hirahara, K. Nakatsuji, F. Komori, Y. Ando, and I. Matsuda, Phys. Rev. B **81**, 041309(R) (2010).

[5] D. Hsieh, Y. Xia, D. Qian, L. Wray, J. H. Dil, F. Meier, J. Osterwalder, L. Patthey, J. G. Checkelsky, N. P. Ong, A. V. Fedorov, H. Lin, A. Bansil, D. Grauer, Y. S. Hor, R. J. Cava, and M. Z. Hasan, Nature **460**, 1101 EP (2009).

[6] Z.-H. Pan, E. Vescovo, A. V. Fedorov, D. Gardner, Y. S. Lee, S. Chu, G. D. Gu, and T. Valla, Phys. Rev. Lett. **106**, 257004 (2011).

[7] K. Miyamoto, A. Kimura, T. Okuda, H. Miyahara, K. Kuroda, H. Namatame, M. Taniguchi, S. V. Eremeev, T. V. Menshchikova, E. V. Chulkov, K. A. Kokh, and O. E. Tereshchenko, Phys. Rev. Lett. **109**, 166802 (2012).

[8] G. Landolt, S. Schreyeck, S. V. Eremeev, B. Slomski, S. Muff, J. Osterwalder, E. V. Chulkov, C. Gould, G. Karczewski, K. Brunner, H. Buhmann, L. W. Molenkamp, and J. H. Dil, Phys. Rev. Lett. **112**, 057601 (2014).

[9] M. Z. Hasan and C. L. Kane, Rev. Mod. Phys. **82**, 3045 (2010).

[10] B. Bradlyn, J. Cano, Z. Wang, M. G. Vergniory, C. Felser, R. J. Cava, and B. A. Bernevig, Science **353** (2016).

[11] B. Q. Lv, H. M. Weng, B. B. Fu, X. P. Wang, H. Miao, J. Ma, P. Richard, X. C. Huang, L. X. Zhao, G. F. Chen, Z. Fang, X. Dai, T. Qian, and H. Ding, Phys. Rev. X **5**, 031013 (2015).

[12] A. A. Soluyanov, D. Gresch, Z. Wang, Q. S. Wu, M. Troyer, X. Dai, and B. A. Bernevig, Nature **527**, 495 (2015).

[13] N. P. Armitage, E. J. Mele, and A. Vishwanath, Rev. Mod. Phys. **90**, 015001 (2018).

[14] S.-Y. Xu, I. Belopolski, N. Alidoust, M. Neupane, G. Bian, C. Zhang, R. Sankar, G. Chang, Z. Yuan, C.-C. Lee, S.-M. Huang, H. Zheng, J. Ma, D. S. Sanchez, B. Wang, A. Bansil, F. Chou, P. P. Shibayev, H. Lin, S. Jia, and M. Z. Hasan, Science **349**, 613 (2015).

[15] N. Hao and J. Hu, National Science Review **6**, 213 (2018).

[16] C. Fang, H. Weng, X. Dai, and Z. Fang, Chinese Physics B **25**, 117106 (2016).

[17] B. Q. Lv, Z.-L. Feng, Q.-N. Xu, X. Gao, J.-Z. Ma, L.-Y. Kong, P. Richard, Y.-B. Huang, V. N. Strocov, C. Fang, H.-M. Weng, Y.-G. Shi, T. Qian, and H. Ding, Nature **546**, 627 (2017).

[18] J.-Z. Ma, J.-B. He, Y.-F. Xu, B. Q. Lv, D. Chen, W.-L. Zhu, S. Zhang, L.-Y. Kong, X. Gao, L.-Y. Rong, Y.-B. Huang, P. Richard, C.-Y. Xi, E. S. Choi, Y. Shao, Y.-L. Wang, H.-J. Gao, X. Dai, C. Fang, H.-M. Weng, G.-F. Chen, T. Qian, and H. Ding, Nature Physics **14**, 349 (2018).

[19] :w
G. W. Winkler, Q. S. Wu, M. Troyer, P. Krogstrup, and A. A. Soluyanov, Phys. Rev. Lett. **117**, 076403 (2016).

[20] S. Zaheer, S. M. Young, D. Cellucci, J. C. Y. Teo, C. L. Kane, E. J. Mele, and A. M. Rappe, Phys. Rev. B **87**, 045202 (2013).

[21] G. W. Winkler, S. Singh, and A. A. Soluyanov, Chinese Physics B **28**, 077303 (2019).

[22] Z. Zhu, G. W. Winkler, Q. S. Wu, J. Li, and A. A. Soluyanov, Phys. Rev. X **6**, 031003 (2016).

[23] D. Di Sante, P. Barone, R. Bertacco, and S. Picozzi, Advanced Materials **25**, 509 (2013).

[24] J. Krempaský, H. Volfová, S. Muff, N. Pilet, G. Landolt, M. Radović, M. Shi, D. Kriegner, V. Holý, J. Braun, H. Ebert, F. Bisti, V. A. Rogalev, V. N. Strocov, G. Springholz, J. Minár, and J. H. Dil, Phys. Rev. B **94**, 205111 (2016).

[25] J. Krempaský, M. Fanciulli, N. Pilet, J. Minár, W. Khan, M. Muntwiler, F. Bertran, S. Muff, A. Weber, V. Strocov, V. Volobuiev, G. Springholz, and J. Dil, Journal of Physics and Chemistry of Solids (2017).

[26] D. Kriegner, G. Springholz, C. Richter, N. Pilet, E. M uller, M. Capron, H. Berger, V. Holý, J. H. Dil, and J. Krempaský, Crystals **9**, 335 (2019).

[27] M. Hoesch, T. Greber, V. N. Petrov, M. Muntwiler, M. Hengsberger, W. Auwärter, and J. Osterwalder, J. Electron Spectrosc. Relat. Phenom. **124**, 263 (2002).

[28] H. Ebert, D. Ködderitzsch, and J. Minár, Rep. Prog. Phys. **74** (2011).

[29] D. Takane, Z. Wang, S. Souma, K. Nakayama, T. Nakamura, H. Oinuma, Y. Nakata, H. Iwasawa, C. Cacho, T. Kim, K. Horiba, H. Kumigashira, T. Takahashi, Y. Ando, and T. Sato, Phys. Rev. Lett. **122**, 076402 (2019).

[30] D. S. Sanchez, I. Belopolski, T. A. Cochran, X. Xu, J.-X. Yin, G. Chang, W. Xie, K. Manna, V. S uss, C.-Y. Huang, N. Alidoust, D. Multer, S. S. Zhang, N. Shumiya, X. Wang, G.-Q. Wang, T.-R. Chang, C. Felser, S.-Y. Xu, S. Jia, H. Lin, and M. Z. Hasan, Nature **567**, 500 (2019).

[31] Z. Rao, H. Li, T. Zhang, S. Tian, C. Li, B. Fu, C. Tang, L. Wang, Z. Li, W. Fan, J. Li, Y. Huang, Z. Liu, Y. Long, C. Fang, H. Weng, Y. Shi, H. Lei, Y. Sun, T. Qian, and H. Ding, Nature **567**, 496 (2019).

[32] J. Krempaský, S. Muff, F. Bisti, M. Fanciulli, H. Volfová, A. P. Weber, N. Pilet, P. Warnicke, F. Bertran, H. Ebert, J. Braun, J. Minár, G. Springholz, J. Dil, and V. Strocov, Nat. Commun. **7**, 13071 (2016).

[33] G. Kremer, T. Jaouen, B. Salzmann, L. Nicolaï, M. Rumo, C. W. Nicholson, B. Hildebrand, J. H. Dil, J. Minár, G. Springholz, J. Krempaský, and C. Monney, Phys. Rev. Research **2**, 033115 (2020).

[34] J. Krempaský, M. Fanciulli, L. Nicolaï, J. Minár, H. Volfová, O. Caha, V. V. Volobuev, J. Sánchez-Barriga, M. Gmitra, K. Yaji, K. Kuroda, S. Shin, F. Komori, G. Springholz, and J. H. Dil, Phys. Rev. Research **2**, 013107 (2020).

[35] P. Zhang, P. Richard, T. Qian, Y.-M. Xu, X. Dai, and H. Ding, Review of Scientific Instruments **82**, 043712 (2011).

[36] F. Meier, J. H. Dil, and J. Osterwalder, New J. Phys. **11**, 125008 (2009).

[37] J. Krempaský, S. Muff, J. Minár, N. Pilet, M. Fanciulli, A. P. Weber, E. B. Guedes, M. Caputo, E. Müller, V. V. Volobuev, M. Gmitra, C. A. F. Vaz, V. Scagnoli, G. Springholz, and J. H. Dil, Physical Review X **8**, 021067 (2018).